RPGR: Deep Phenotyping and Genetic Characterization With Findings Specific to the 3′-end of ORF15

Matthew D. Benson, Souvick Mukherjee, Aime R. Agather, Delphine Blain, Denise Cunningham, Robert Mays, Xun Sun, Tiansen Li, Robert B. Hufnagel, Brian P. Brooks, Laryssa A. Huryn, Wadih M. Zein, and Catherine A. Cukras

National Eye Institute, National Institutes of Health, Bethesda, Maryland, United States

Correspondence: Catherine A. Cukras, Unit on Clinical Investigation of Retinal Disease, National Eye Institute, National Institutes of Health, Building 10-CRC Room 10C438, Bethesda, MD 20892-1204, USA; cukrasc@nei.nih.gov.

Received: December 30, 2022
Accepted: July 27, 2023
Published: September 11, 2023

Citation: Benson MD, Mukherjee S, Agather AR, et al. *RPGR*: Deep phenotyping and genetic characterization with findings specific to the 3′-end of ORF15. *Invest Ophthalmol Vis Sci.* 2023;64(12):19. https://doi.org/10.1167/iovs.64.12.19

Purpose. To describe a group of patients with retinitis pigmentosa GTPase regulator (*RPGR*)-related retinopathy with a tapetal-like retinal sheen and corresponding changes in the reflectivity of the ellipsoid zone on optical coherence tomography (OCT) imaging.

Methods. A retrospective case series of 66 patients with a disease-causing variant in *RPGR* was performed. An expert examiner, masked to patient demographics, clinical evaluations, and specific *RPGR* variant, analyzed color fundus photographs for the presence of a tapetal-like retinal sheen and assessed OCT images for the presence of an abnormally broad hyper-reflective band in the outer retina. Longitudinal reflectivity profiles were generated and compared with healthy controls.

Results. Twelve patients (18.2%) had a retinal sheen on color images that cosegregated with an abnormally broad hyper-reflective ellipsoid zone band on OCT imaging. Three-fourths of these patients were male, had a cone–rod dystrophy, and had pathogenic *RPGR* variants located toward the 3′-end of ORF15. This group had a different longitudinal reflectivity profile signature compared with controls. After a period of prolonged dark adaptation, the abnormal hyper-reflective band on OCT became less apparent, and the outer retinal layers adopted a more normal appearance.

Conclusions. *RPGR*-related retinopathy should be considered for males presenting with retinal sheen, abnormal ellipsoid zone hyper-reflectivity, and cone or cone–rod dysfunction on ERG, and pursued with molecular testing. Our results have implications for understanding the role of the C-terminal domain encoded by RPGR ORF15 in the phototransduction cascade. Further, the findings may be important to incorporate into both inclusion criteria and outcome measure developments in future *RPGR*-related cone or cone–rod dystrophy clinical trials.

Keywords: *RPGR*, cone–rod dystrophy, tapetal reflex, retinal sheen, longitudinal reflectivity profile

Pathogenic variants in the retinitis pigmentosa GTPase regulator (*RPGR*) gene represent an important cause of vision loss, accounting for nearly 5% of all instances of retinal degeneration.[1] Located on chromosome Xp21.1, *RPGR* has several alternatively spliced isoforms with the retina-specific open reading frame 15 ($RPGR^{ORF15}$) being the major isoform implicated in retinal disease. The $RPGR^{ORF15}$ isoform contains a highly repetitive purine-rich region within the terminal exon 15 (ORF15) and encodes a glycine- and glutamate-rich domain. This 567 amino acid-containing region has been identified as a mutational hot spot and accounts for approximately 60% of all *RPGR* cases.[2] Localized to the base of the connecting cilium of rod and cone photoreceptors, RPGR interacts with several proteins that have roles in ciliary trafficking and phototransduction, including RPGRIP1, PDE6D, CEP290, and TTLL5, among others.[3–8] Given its localization and binding partners, RPGR is believed to function more broadly in microtubule-based intraflagellar transport and trafficking of vesicles between the inner and outer segments of photoreceptors.[6,7] The precise mechanism(s) by which this occurs, and the identity of these cargoes remains to be elucidated.

More than two-thirds of patients with *RPGR*-related retinopathy have a severe, early-onset form of X-linked rod–cone dystrophy (RCD).[9] These patients typically present with nyctalopia and peripheral vision loss in childhood and subsequently develop legal blindness, often by their fifth decade of life.[10] The remaining subset of patients present with a CD or cone–rod dystrophy (CRD) and initially develop symptoms of central vision loss, dyschromatopsia, and photophobia in their third or fourth decade of life.[11] In some cases, progressive rod dysfunction ensues.[11]

Given the variation in disease presentation and progression in patients with *RPGR*-related RCD and CRD,[9] deep phenotyping becomes crucial for both improving diagnostic accuracy and understanding disease mechanisms. This factor is especially important when considering patient eligibility

and establishing outcome measures in interventional clinical trials for *RPGR*-related retinopathy.

A tapetal-like fundus reflex has been described as a characteristic feature in female *RPGR* carriers[12–16]; however, an abnormal fundus reflex has rarely been reported in hemizygous males.[17] To further investigate this constellation of findings, we report on a series of 66 patients with *RPGR*-related retinopathy and evaluate specific multimodal imaging findings, full-field ERG patterns, and genotypes to further elucidate genotype–phenotype associations.

Methods

Study Design

We performed a single-center retrospective review of patients ($n = 82$) from ages 1 to 78 years with molecularly confirmed *RPGR*-related retinopathy who were evaluated at the National Eye Institute, National Institutes of Health, in Bethesda, Maryland, before December 2021. Each patient consented to participating in a clinical research protocol at the National Eye Institute as part of screening protocols, genotyping protocols, and/or natural history protocols for retinal diseases or other ocular conditions. This retrospective study, "Deep Phenotyping *RPGR* Retinopathy," was sponsored by the National Institutes of Health. Institutional review board (IRB)/Ethics Committee approval was obtained (IRB #001134) and consent to this retrospective data analysis was waived. Healthy control patients ($n = 7$) who consented to participate in "A Survey study of Retinitis Pigmentosa (RP) clinical measures and repeatability testing of potential outcome measures" (19-EI-0056), which received IRB approval, were included as a comparison group for quantitative optical coherence tomography (OCT) analyses. All

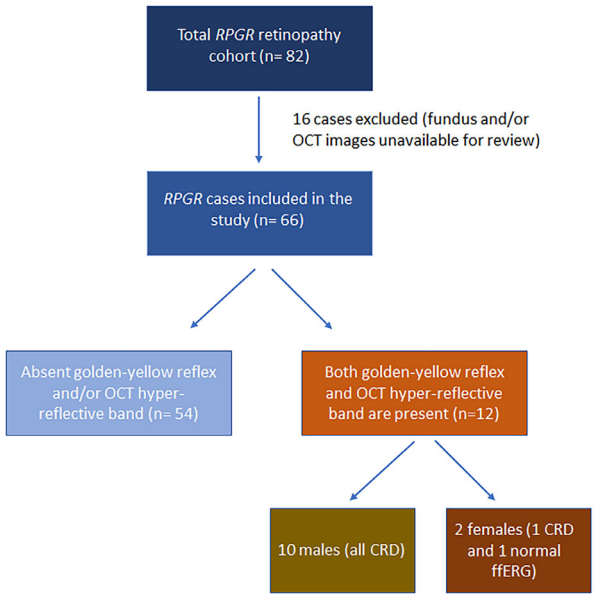

Figure 1. Flow diagram of the study design and primary results. Of the *RPGR*-related retinopathy cases meeting the inclusion criteria, 12 (18.2%) demonstrated both the tapetal-like retinal sheen and an abnormally broad hyper-reflective band in the outer retina on OCT imaging.

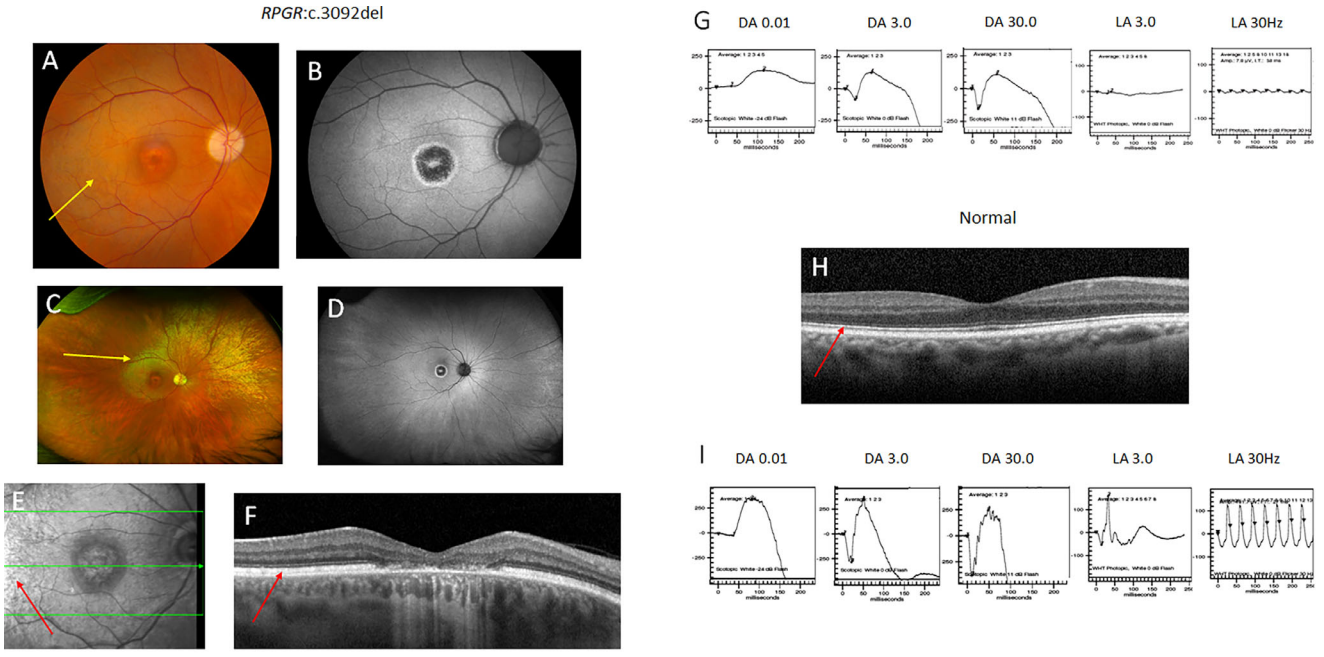

Figure 2. Conventional flash-based fundus photograph demonstrating the tapetal-like retinal sheen (*yellow arrow*) (**A**) in a 47-year-old male with CRD and the pathogenic variant *RPGR*:c.3092del (**A–G**). Topcon fundus autofluorescence imaging reveals a bullseye pattern with foveal hypoautofluorescence and a surrounding rim of hyper-autofluorescence (**B**). Optos UWF fundus photography, captured with red (635 nm) and green (532 nm) lasers, reveals a tapetal-like reflex with a greenish hue (**C**). Optos fundus autofluorescence imaging demonstrates a bullseye pattern of foveal hyper- and hypoautofluorescence (**D**). En face near-infrared reflectance image (**E**) and SD-OCT B-scan image (**F**) illustrate abnormal hyper-reflectivity that localizes to the EZ (*red arrow*) and corresponds with the greenish reflex apparent on pseudocolor fundus photography. The patient's full-field ERG photopic responses are diminished to a greater degree than the scotopic responses, consistent with a CRD phenotype (**G**). OCT B-scan image from a healthy 47-year-old man (with no known ocular disease) demonstrating normal macular architecture without evidence of the abnormal hyper-reflective outer retinal band (**H**). A normal ERG is presented for reference (**I**). DA, dark adapted; LA, light adapted. Stimulus intensities are displayed in units of cd•s/m^2.

Investigative Ophthalmology & Visual Science

study procedures conformed to the principles established in the Declaration of Helsinki.

Data Collection

Of the 82 patients with *RPGR*-related retinopathy, patient records were reviewed for presence of Topcon color fundus imaging (Topcon Medical Systems, Oakland, NJ) using the OIS digital imaging system (OIS WinStation, Sacramento, CA) and OCT imaging with either Spectralis (Heidelberg Engineering, Heidelberg, Germany) or Cirrus (Carl Zeiss Meditec, Dublin, CA) devices. Where available, Optos ultra-widefield (UWF) confocal scanning laser ophthalmoscopy images were also reviewed using the OptosAdvance software (Optos, Dunfermline, Scotland, UK).

Sixteen patients were found not to have both imaging modalities and were, therefore, excluded from subsequent analyses (Fig. 1). For the remaining 66 cases, patient demographics were retrieved and included age at the most recent examination and sex. Best-corrected visual acuity (BCVA), converted to logMAR notation, was also recorded from the most recent visit. LogMAR values for acuities of <20/800 were based on estimates from Schulze-Bonsel et al (2006).[18] Disease-causing variants in *RPGR* were documented and both hemizygous males and heterozygous females were included in this study.

Full-field ERG, performed according to the International Society for Clinical Electrophysiology of Vision standards,[19] was reviewed for each patient, where available. If the scotopic responses were reduced and delayed to a greater degree than the photopic responses, the ERG phenotype was designated as RCD. A patient was identified as having a CD or CRD if only the photopic responses were diminished or if the photopic responses were more affected than the scotopic responses, respectively. An ERG was consid-

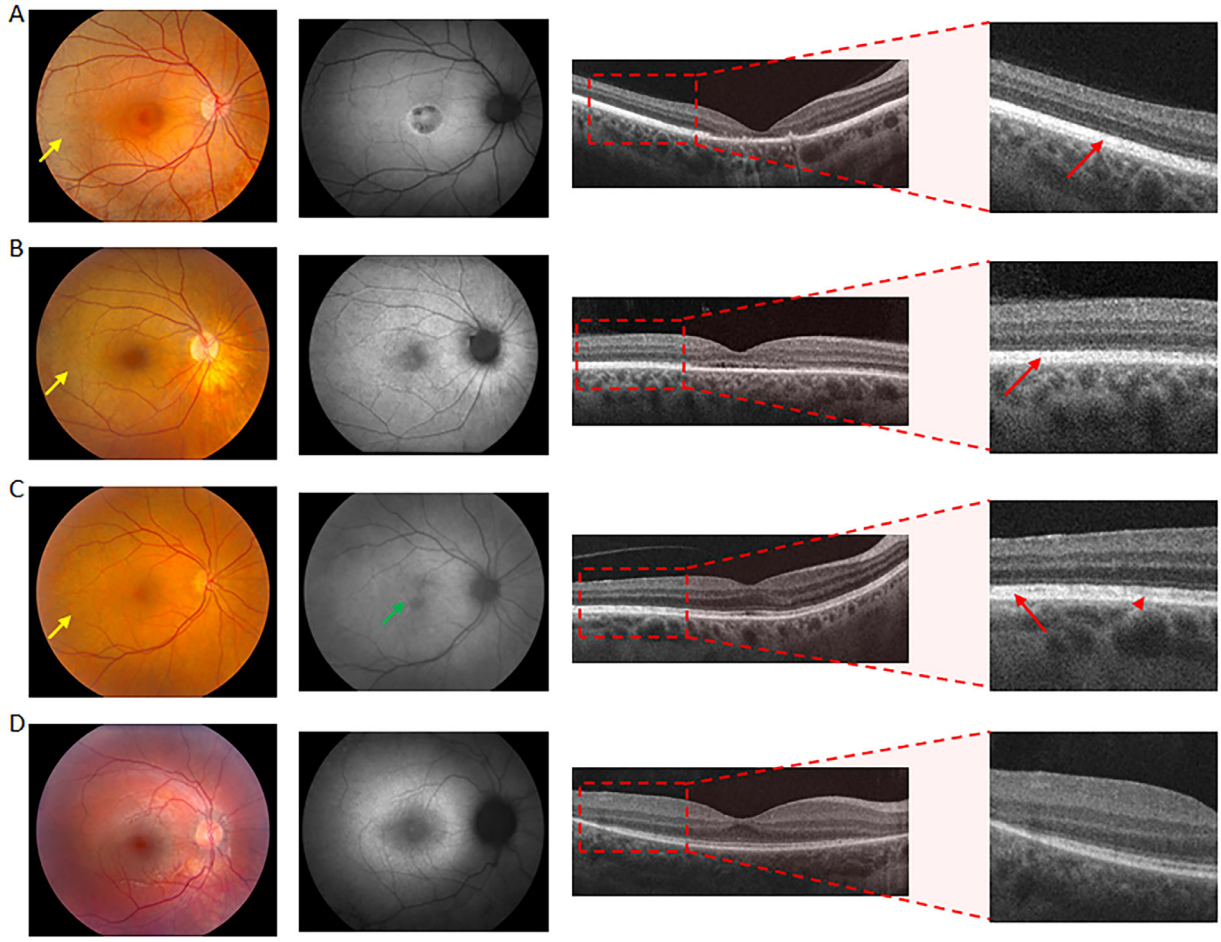

Figure 3. True color fundus photographs depicting the tapetal-like retinal sheen (*yellow arrow*) in a 44-year-old man with CRD and the pathogenic variant *RPGR*:c.3092del (**A**). Fundus autofluorescence imaging displaying foveal hypoautofluorescence with surrounding hyperautofluorescence. Corresponding OCT demonstrating the parafoveal region where the image was cropped (*dashed box*) and subsequently evaluated by an expert examiner. An abnormally broad hyper-reflective band in the EZ (*red arrow*) is apparent in this case (**A**). A retinal sheen (*yellow arrow*) and corresponding abnormally hyper-reflective band in the outer retina on OCT (*red arrow*) are also apparent in a 47-year-old man with CRD and the pathogenic variant *RPGR*:c.3039_3040del (**B**). Fundus autofluorescence imaging reveals perifoveal hyperautofluorescence. In addition, he has significant foveal thinning with subfoveal EZ loss, consistent with his CRD phenotype (**B**). More subtle retinal sheen (*yellow arrow*) in a 64-year-old female carrier with CRD and the pathogenic variant *RPGR*:c.3092del (**C**). Her fundus autofluorescence imaging reveals subtle perifoveal hyperautofluorescent changes (*green arrow*). She has subtle variegated and nonconfluent areas of abnormally hyper-reflective outer retinal layers on OCT (*red arrow*) interspersed with more normal-appearing outer retinal layers (*red arrowhead*) (**C**). A 10-year-old boy with RCD and the pathogenic variant *RPGR*:c.2236_2237del does not appear to have a retinal sheen (**D**). Fundus autofluorescence imaging reveals a distinct perifoveal ring of hyperautofluorescence. His OCT demonstrates outer retinal thinning with preserved subfoveal outer nuclear layer and EZ (**D**).

Investigative Ophthalmology & Visual Science

ered nonrecordable if there were no discernible scotopic or photopic responses.

Case Identification

An expert examiner (CAC), who was masked to patient demographics, clinical evaluations, and the specific *RPGR* variant, assessed bilateral conventional flash-based fundus camera photographs for the presence of a tapetal-like retinal sheen (Figs. 2 and 3, *yellow arrows*) and a limited area (approximately 1 mm in width centered around a distance of 3 mm temporal to the fovea) of the paracentral spectral domain OCT B-scans for the presence of an abnormally broad hyper-reflective band in the ellipsoid zone (EZ) area of the outer retina (Figs. 2 and 3, *red arrows*). The OCT B-scans were cropped to include the paracentral macular region and exclude the fovea (Fig. 3A, *dashed box* represents the approximated area of the OCT that was cropped and presented to the expert examiner) in an effort to reduce the ability of the examiner to ascertain the presence of a RCD or CRD ERG phenotype a posteriori.

Longitudinal Reflectivity Profiles (LRPs)

To enhance visualization and facilitate quantification of the abnormal hyper-reflective EZ band identified on OCT, we generated LRPs from Spectralis OCT B-scans. Of the 10 males in our cohort with retinal sheen and abnormal hyper-reflectivity, seven had Spectralis images available for analysis (the remaining three had Cirrus OCT images only). First, a test spot or location at approximately 3 mm temporal to the foveal center was chosen for each foveal B-scan. This location was selected to avoid regions of foveal atrophy. The individual B-scans were then manually rotated such the marked test spot tangentially contacted the horizontal straight line, without any resizing or interpolation. A horizontal test strip centered around the test spot having a total width of 10 pixels (corresponding to 117.4 µm in Spectralis) was programmed to traverse through each of the retinal layers, and the normalized reflectivity (ranged 0–1 within the B-scan) and position of the test strip (in pixels) was recorded for each pixel of movement. From this, the LRP was generated and presented graphically to illustrate the relative reflectivity peaks and troughs, denoting the retinal layers and boundaries, which exist when traversing through the retina in each B-scan.

OCT Changes Observed With Dark Adaptation

The tapetal-like retinal sheen and OCT changes identified in our *RPGR* cohort were reminiscent of the features present in Oguchi disease, a form of congenital stationary night blindness with impaired inactivation of photoactivated rhodopsin.[20–22] To assess whether the appearance of the abnormally broad hyper-reflective band on OCT changed after a period of prolonged dark adaptation (similar to the changes known as the Mizuo–Nakamura phenomenon), we patched an eye ($n = 1$) of a 38-year-old man with *RPGR* CRD for 2 hours and compared the initial light-adapted appearance of the outer retinal layers with the dark-adapted appearance on registered OCT scans captured immediately after the patch was removed.

Statistical Analysis

Basic descriptive statistics were computed in Microsoft Excel. Comparisons for statistical significance were performed using the nonparametric Mann–Whitney *U* test. Graphs were generated in GraphPad Prism 9.5.1.

Results

Patient Characteristics

Of the 66 patients with both color fundus imaging and OCT available for review, the presence of both a tapetal-like retinal sheen and a broad hyper-reflective band in the outer retina on paracentral macular OCT scans were identified in 12 patients (18.2%) (Fig. 1). These included 10 hemizygous males, two of whom were siblings (patients 4 and 5), and two heterozygous females (Table 1). One of the *RPGR* female carriers (patient 6) was the mother of one of the hemizygous males (patient 7) (Table 1). There were no instances where a patient had either the retinal sheen or the OCT hyper-reflectivity, but not both features. The remaining 54 patients did not have either a retinal sheen or an abnormal hyper-reflective band on OCT imaging. Instead, 51 (94.4%) had evidence of outer retinal thinning on OCT, and three (5.6%) heterozygous females had normal OCT scans (Table 2).

The median age at the most recent examination of patients with the retinal sheen and OCT changes was 47.0 years (range, 14–64 years) compared with 33.5 years (range, 9–68 years) in the group without these findings ($P = 0.08$). The logMAR BCVA was not significantly different

Table 1. Patients Manifesting a Tapetal-Like Retinal Sheen and Outer Retinal Hyper-Reflectivity on OCT

Patient	Sex	Age at Last Examination (Years)	LogMAR BCVA (OD, OS)	ERG Phenotype	Pathogenic *RPGR* Variant
1	Male	14	0.30, 0.20	CRD	c.2405_2406del (p.E802Gfs*32)
2	Male	38	0.50, 1.00	CRD	c.2986G>T (p.E996*)
3	Male	47	0.90, 0.80	CRD	c.3039_3040del (p.E1014Gfs*64)
*4	Male	59	0.80, 0.90	CRD	c.3058G>T (p.E1020*)
*5	Male	58	1.00, 1.00	CRD	c.3058G>T (p.E1020*)
†6	Female	64	0, 0	CRD	c.3092del (p.E1031Gfs*58)
†7	Male	44	0.50, 0.60	CRD	c.3092del (p.E1031Gfs*58)
8	Male	47	0.30, 0.30	CRD	c.3092del (p.E1031Gfs*58)
9	Female	58	–0.10, 0	Normal	c.3096_3097del (p.E1033Rfs*45)
10	Male	42	0.50, 0.20	CRD	c.3164del (p.N1055Tfs*34)
11	Male	36	0.50, 1.00	CRD	c.3179_3183del (p.E1060Gfs*17)
12	Male	47	0.40, 1.51	CD	c.3255del (p.Y1085*)

* Patients 4 and 5 are siblings.
† Patients 6 and 7 are mother and son.

Investigative Ophthalmology & Visual Science

Table 2. Baseline Demographics and Clinical Characteristics of *RPGR*-Related Retinopathy Cohort

***RPGR* Cohort Characteristics ($n = 66$)**	**Retinal Sheen Present ($n = 12$)**	**Retinal Sheen Absent ($n = 54$)**
Sex		
Male	10 (83.3)	39 (72.2)
Female	2 (16.7)	15 (27.8)
Age (years)	47.0 (14.0–64.0)	33.5 (9.0–68.0)
BCVA (logMAR)	0.65 (0–1.0)	0.50 (0–2.30)
Full-field ERG pattern		
NR	0	16 (29.6)
RCD	0	21 (38.9)
CRD	10 (83.3)	6 (11.1)
CD	1 (8.3)	0
Normal	1 (8.3)	3 (5.6)
NA	0	8 (14.8)
OCT perifoveal appearance		
Abnormally hyper-reflective outer retinal band	12 (100)	0
Outer retinal thinning	0	51 (94.4)
Normal	0	3 (5.6)

NR, nonrecordable; NA = not available.
Values are number (%) or median (range).
There was no significant difference in age ($P = 0.08$) or BCVA ($P = 0.88$) between the retinal sheen present or absent groups.

between those with (median, 0.65; range, 0–1) and without (median, 0.50; range, 0–2.3) the retinal sheen and OCT changes ($P = 0.88$) (Table 2). Because both of these groups included different proportions of heterozygous females, we also compared the age and logMAR BCVA of hemizygous males only because they generally have a more severe retinal disease than female carriers. Similar to the combined male and female groups, there was no significant difference in the age of male patients with (median, 45.5 years; range, 14–59 years) and without (median, 28.0 years; range, 9–68 years) the retinal sheen and OCT changes ($P = 0.29$). Likewise, there was no significant difference in logMAR BCVA between those with (median, 0.75; range, 0–1) and without (median, 0.60; range, 0.1–2.3) these features ($P = 0.67$; data not shown).

Of the 12 patients with a tapetal-like retinal sheen and abnormal outer retinal hyper-reflectivity on OCT, the vast majority had a CRD (10 patients [83.3%]) or CD (1 patient [8.3%]) ERG phenotype (Table 2). One female *RPGR* carrier had an ERG within normal limits. Of the 54 patients without a retinal sheen or OCT changes, the majority had either a RCD (21 patients [38.9%]) or nonrecordable (16 patients [29.6%]) ERG. Six of these 54 patients (11.1%) had a CRD phenotype, and three were heterozygous females with a normal ERG (Table 2).

Tapetal-Like Retinal Sheen and Corresponding OCT Hyper-Reflectivity

The location of the tapetal-like retinal sheen on conventional flash-based fundus camera imaging (Fig. 2A) corresponded to the area of the abnormally broad hyper-reflective band in the EZ area on OCT (Figs. 2E and 2F), as demonstrated in a 47-year-old man with *RPGR*:c.3092del (patient 8). Figure 2G depicts a normal OCT macula from a 47-year-old man who has no known ocular disease. This normal OCT illustrates the typical hyper-reflective EZ and RPE interdigitation zone/RPE bands separated by a hyporeflective space that corresponds with the region of the photoreceptor outer segments.[23] The retinal sheen in the same *RPGR* patient imaged with UWF confocal scanning laser ophthalmoscopy demonstrated a tapetal-like appearance of the reflex with a greenish hue (Fig. 2C). Fundus autofluorescence imaging confirmed a bullseye-like pattern of foveal hypo- and hyperautofluorescence (Figs. 2B and 2D). The distribution of the retinal sheen evident with conventional fundus imaging (Fig. 2J) coincided with the distribution of the greenish reflex in the macula apparent with UWF imaging (Fig. 2K). This patient lacked any overt signs of vascular attenuation, pigment deposition, or peripheral retinal pathology. The full-field ERG illustrates that the patient's photopic responses are more reduced and delayed compared with the scotopic responses, consistent with a CRD phenotype (Fig. 2H). Figure 2I demonstrates normal ERG responses for reference.

Figure 3A presents an example of the multimodal imaging findings in a 44-year-old man with *RPGR*:c.3092del (patient 7) exemplifying the paramacular tapetal-like retinal sheen (*yellow arrow*) and, on OCT, an abnormally broad hyper-reflective EZ in the parafoveal area (*red arrow*). A region (*dashed box*) that is representative of where the OCT images had been cropped and subsequently evaluated by an expert examiner is demonstrated. Fundus autofluorescence imaging reveals foveal hypoautofluorescence with surrounding hyperautofluorescence. In addition, his OCT revealed significant foveal thinning and subfoveal EZ loss, consistent with his CRD phenotype.

A similar retinal sheen (*yellow arrow*) and OCT findings (*red arrow*) were evident in a 47-year-old man with *RPGR*:c.3039_3040del and CRD (patient 3; Fig. 3B). He also had evidence of subfoveal EZ disruption and perifoveal hyper-autofluorescence. Figure 3C highlights the subtle retinal sheen (*yellow arrow*) and OCT hyper-reflectivity in a 64-year-old heterozygous female with *RPGR*:c.3092del and CRD (patient 6). She had subtle variegated areas of abnormally hyper-reflective outer retinal layers on OCT (*red arrow*) with adjacent areas of more normal appearing outer retinal structures (*red arrowhead*), presumably resulting from random X-chromosome inactivation. Her fundus autofluorescence imaging revealed subtle perifoveal hyperautofluorescent changes (*green arrow*). Neither the retinal sheen nor the abnormal OCT hyper-reflectivity was apparent in a 10-year-old boy with *RPGR*:c.2236_2237del (Fig. 3D). Instead, he had evidence of perimacular outer nuclear layer and EZ

Investigative Ophthalmology & Visual Science

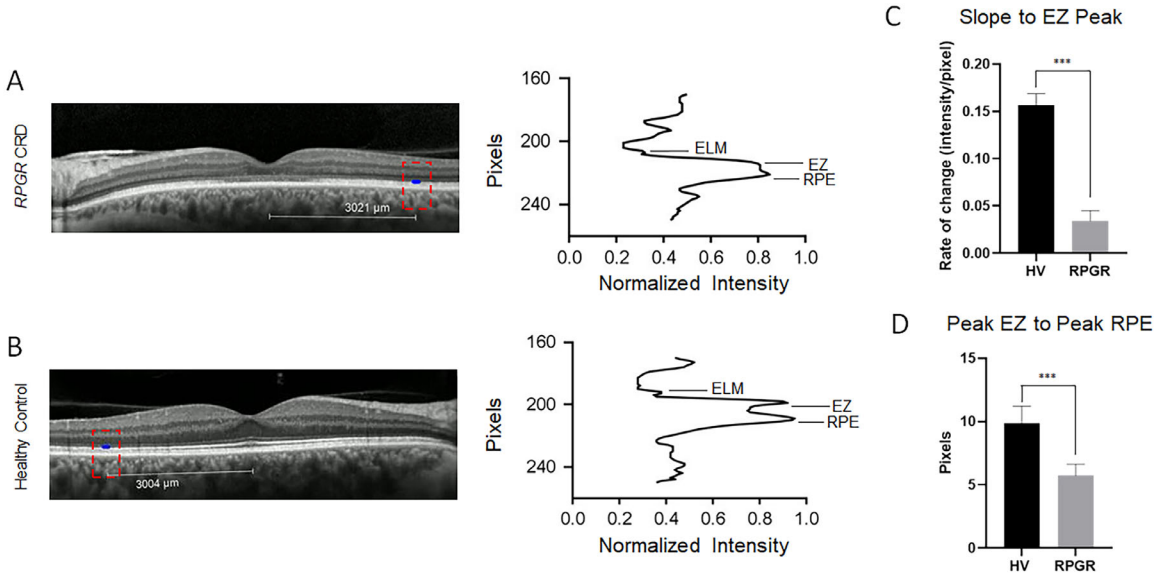

Figure 4. A comparison of the LRPs of male *RPGR* CRD patients ($n = 14$ eyes) with healthy controls ($n = 14$ eyes) (**A** and **B**). The *dashed box* indicates the area on the OCT B-scan that corresponds with the LRP signals. The horizontal blue bar (shown at the level of the EZ) is programmed to traverse the retina vertically and measure intensity signals at each pixel. Representative LRP of a 47-year-old man with CRD and the pathogenic variant *RPGR*:c.3039_3040del demonstrates a broad EZ band and absence of a substantial intensity trough between the EZ and RPE (**A**) compared with a healthy control (**B**). The slope of the EZ profile, measured in the interval beginning 5 pixels before the EZ intensity peak to the EZ peak, was significantly smaller in the *RPGR* CRD patients (median, 0.036 intensity/pixel; range, 0.020–0.058) compared with healthy controls (median, 0.16 intensity/pixel; range, 0.14–0.18) ($P < 0.0001$) (**C**). The distance between the EZ intensity peak and RPE intensity peak was smaller in the *RPGR* CRD cohort (median, 6.0 pixels; range, 4.0–7.0) compared with controls (median, 10.0 pixels; range, 6.0–11.0) ($P < 0.0001$) (**D**).

thinning on OCT with a perifoveal ring of hyperautofluorescence. His clinical examination demonstrated significant degenerative changes in the retina beyond the boundaries of the color fundus image, consistent with his RCD ERG phenotype.

LRPs With Quantitative Metrics Compared With Healthy Controls

The outer retinal LRP signature in the male *RPGR* CRD patients ($n = 14$ eyes; OCT of patient 3 demonstrated) with retinal sheen demonstrated a broadened area of increased intensity or reflectivity between the EZ and RPE bands relative to healthy controls ($n = 14$ eyes; one male and six females) (Figs. 4A and 4B). The rise or slope of the EZ profile, measured in the interval beginning five pixels before the EZ intensity peak to the EZ peak (intensity/pixel), was significantly smaller in the *RPGR* CRD patients (median, 0.036; range, 0.020–0.058) compared with healthy controls (median, 0.16; range, 0.14–0.18) ($P < 0.0001$) (Fig. 4C). In addition, the distance (in pixels) between the EZ intensity peak and RPE intensity peak was smaller in the *RPGR* CRD cohort (median, 6.0; range, 4.0–7.0) compared with controls (median, 10.0; range, 6.0–11.0; $P < 0.0001$) (Fig. 4D).

The minimum EZ intensity, defined as the minimum intensity value in the region between the EZ peak and RPE peak, relative to the EZ and RPE peaks were both larger in the *RPGR* CRD cohort compared with controls (Supplementary Table 1) ($P < 0.0001$ for each). There was no difference in the distance between the ELM and RPE peaks between the two groups (Supplementary Table 1) ($P = 0.29$). The median age of patients with LRPs quantitated in the *RPGR* CRD cohort (median, 47 years; range, 36–59 years) did not differ significantly from the control group (median, 32 years; range, 24–58 years) ($P = 0.10$).

RPGR^{ORF15} Variant Analysis

All 12 patients with a tapetal-like retinal sheen and abnormal OCT hyper-reflectivity were found to have pathogenic variants in exon 15 (ORF15) of *RPGR*^{ORF15} (NM_001034853.2). Three patients had nonsense variants and the remainder had small exonic deletions (Table 1). All nine unique pathogenic *RPGR* variants identified in the 12 patients were either nonsense or frameshift variants. These variants would be predicted to escape nonsense-mediated mRNA decay and instead lead to protein truncation because they all occur in the terminal exon of *RPGR*^{ORF15}. Figure 5 demonstrates the distribution of *RPGR*^{ORF15} variants in patients with (*red arrows*) and without (*grey arrows*) the retinal sheen and OCT changes. In patients with the retinal sheen and OCT changes, pathogenic *RPGR* variants tended to cluster toward the 3′-end of the transcript (Fig. 5).

Changes in OCT Appearance After Prolonged Dark Adaptation

The tapetal-like retinal sheen or greenish reflex on true color or laser-based UWF imaging, respectively, and the corresponding OCT appearance was reminiscent of features of Oguchi disease, an atypical form of congenital stationary night blindness with impaired inactivation of photoactivated rhodopsin.[20–22] Patients with Oguchi disease classically manifest the Mizuo–Nakamura phenomenon where

Investigative Ophthalmology & Visual Science

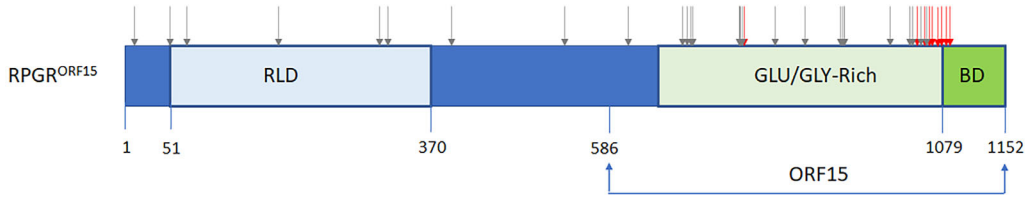

Figure 5. Schematic of the RPGR^{ORF15} protein is illustrated with the major domains highlighted. The *red arrows* indicate pathogenic *RPGR* variants associated with the tapetal-like retinal sheen and outer retinal hyper-reflectivity on OCT imaging. These variants cluster toward the C-terminus of the protein, consistent with an *RPGR* CRD phenotype. The grey arrows indicate pathogenic *RPGR* variants that are not associated with a retinal sheen or hyper-reflective OCT changes. BD, basic domain.

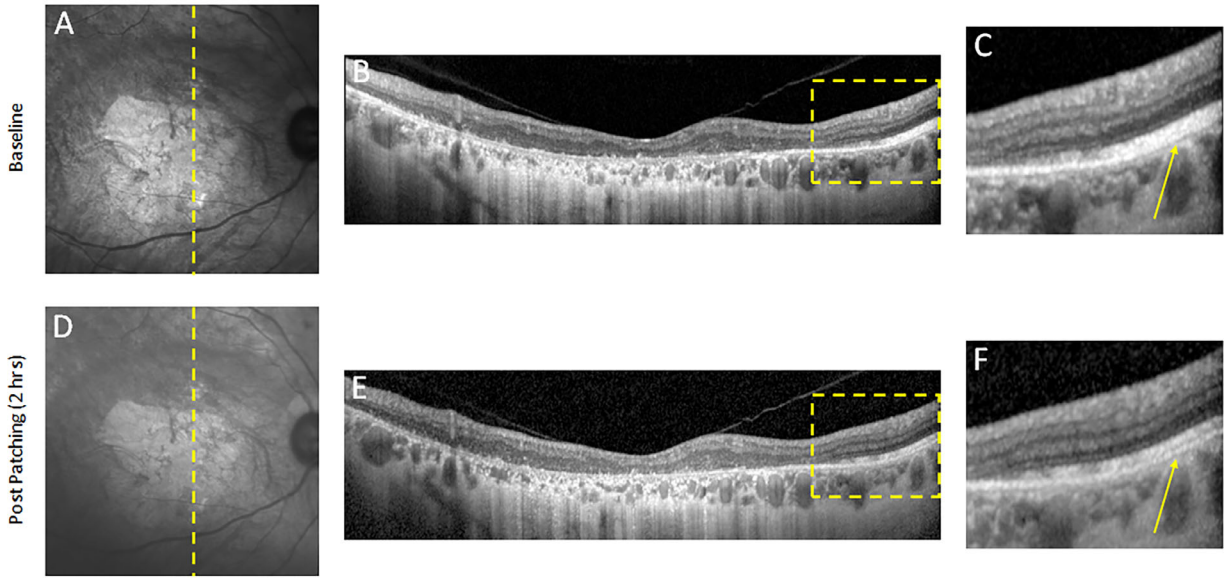

Figure 6. Baseline en face near-infrared reflectance image and OCT B-scan obtained in a light-adapted state of a 38-year-old man with *RPGR*:c.2986G>T CRD (**A–C**). Given the horizontally extensive macular atrophy, vertical OCT B-scans were used and confirmed the abnormally broad hyper-reflective outer retinal band (**A–C**). After a 2-hour period of dark adaptation, the abnormal band is less apparent on a corresponding registered OCT B-scan, and the outer retinal layers adopt a more normal configuration (**D–F**).

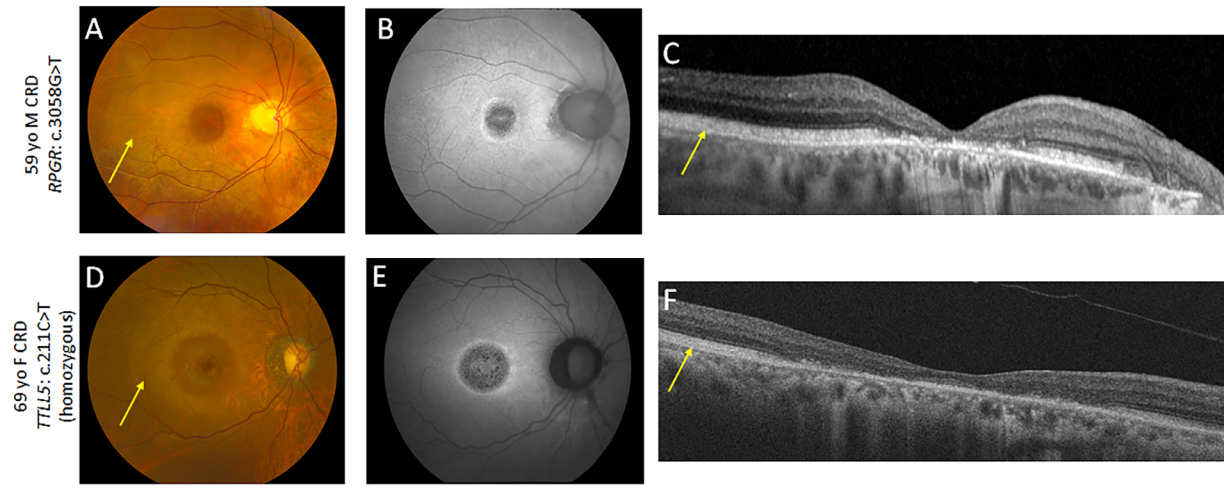

Figure 7. A comparison of the fundus and OCT features in patients with *RPGR* CRD and *TTLL5* CRD. A 59-year-old man with *RPGR*:c.3058G>T CRD manifests the tapetal-like retinal sheen (*arrow*) (**A**), foveal hypoautofluorescence with a surrounding rim of hyperautofluorescence (**B**), and an abnormally hyper-reflective outer retinal band on OCT (*arrow*) (**C**). A 69-year-old woman with homozygous *TTLL5*:c.211C>T CRD has a very similar phenotype with both the retinal sheen and corresponding OCT changes present (**D–F**).

Investigative Ophthalmology & Visual Science

the abnormal fundus reflex disappears after a period of prolonged dark adaptation. At baseline, where the fundus was in a state of normal light adaptation, the abnormally broad hyper-reflective outer retinal band was evident on OCT imaging in a 38-year-old man with *RPGR*:c.2986G>T CRD (patient 2) (Figs. 6A, 6B, and 6C). After a 2-hour period of dark adaptation, the abnormally hyper-reflective band became less apparent, and the outer retinal layers adopted a more normal configuration (Figs. 6D, 6E, and 6F).

RPGR CRD Phenocopies *TTLL5*-Related Retinopathy

Given that the vast majority of our cases with a tapetal-like retinal sheen and OCT hyper-reflectivity had a CRD with pathogenic *RPGR* variants occurring toward the 3′-end of the transcript, we compared this phenotype with that of a patient with pathogenic variants in TTLL5-a protein that interacts with the C-terminal end of *RPGR*[8,24] (Fig. 5). Figure 7 compares the color fundus images, fundus autofluorescence, and OCT findings in a 59-year-old man with a CRD and pathogenic variant in *RPGR* (c.3058G>T; patient 4) (Figs. 7A B, and 7C) to a 69-year-old woman with a CRD and homozygous variants in *TTLL5* (c.211C>T, p.R71*) (Figs. 7D, 7E, 7F). Similar to the *RPGR* CRD case, the patient with *TTLL5*-related retinopathy manifested a retinal sheen surrounding an area of foveal atrophy that was hypoautofluorescent (Figs. 7D and 7E). In addition, an abnormally hyper-reflective outer retinal band was also apparent on OCT imaging (Fig. 7F).

Discussion

We identified a tapetal-like retinal sheen and a corresponding abnormally broad hyper-reflective outer retinal band on OCT in nearly one-fifth of our *RPGR*-related retinopathy cohort. Intriguingly, the vast majority of these cases were males, had a CRD ERG phenotype, and had a pathogenic *RPGR* variant located near the 3′-end of the *RPGR*^{ORF15} transcript, as has been previously highlighted in patients with *RPGR* CRD.[25,26] We propose that, for male patients presenting for clinical evaluation who demonstrate a similar retinal sheen and hyper-reflectivity on OCT, an a posteriori diagnosis of *RPGR*-related CD/CRD should be considered and pursued with molecular testing.

Heckenlively and Weleber (1986)[27] described an X-linked CD in five patients from two families. Interestingly, these patients had a tapetal-like fundus sheen that reportedly seemed to arise from the level of the retinal pigment epithelium.[27] Prolonged dark adaptation resulted in the fundi adopting a more normal reddish-orange appearance, consistent with the Mizuo–Nakamura phenomenon. Similarly, Jacobson et al (1989)[28] reported the clinical features of a four-generation X-linked CD (COD1) family that included a tapetal-like reflex in affected males. Subsequent studies further refined the COD1 locus and identified variants in *RPGR*^{ORF15} as causative.[25,29,30] The tapetal-like fundus features previously described[27,28] are strikingly similar to those that we identified in our *RPGR* patients.

Although a tapetal-like fundus reflex has been well-described in female *RPGR* carriers,[12–16] a similar reflex in male *RPGR* CRD patients has not been as well-characterized.[31–33] We found the retinal sheen to be more apparent in certain patients (Fig. 3A) compared with others (Fig. 3B), and this finding may depend on factors such as patient positioning, the intensity or incident angle of the camera flash, the white balance of the camera, and patient-specific disease aspects, among others. Indeed, in several instances, the presence of the sheen only became evident retrospectively when we identified the presence of the abnormally broad hyper-reflective outer retinal band on OCT and correlated this with the fundus features (Figs. 2A, 2E, 2F). In addition, the red and green laser-based imaging system employed by the UWF camera generated a more tapetal-like reflex with a greenish hue that was often more recognizable than the more subtle retinal sheen generated by the conventional flash-based fundus camera that uses full-spectrum white light (Figs. 2J and 2K). With the broader use of laser-based UWF imaging coupled with a heightened awareness of the possibility of a tapetal-like retinal sheen in *RPGR* CRD patients, we suspect more cases like ours will come to light.

The presence of the abnormally broad hyper-reflective band in the EZ area of the outer retina represents a relatively novel finding in our *RPGR* cohort, particularly for male CRD patients. These patients had a distinctive LRP signature that consisted of a broadened area of reflectivity between the EZ and RPE compared with healthy controls (Figs. 4A and 4B). Quantitative metrics supported this observation and demonstrated a reduced slope of the EZ profile ($P < 0.0001$) and reduced distance between the EZ peak and RPE peak ($P < 0.0001$), both indicating a broader EZ band that did not have the rapid rise and early peak of the EZ profile of the controls (Figs. 4C and 4D). Although the band of EZ reflectivity was broader in the *RPGR* CRD cohort, the overall distance between the ELM and RPE was similar to controls ($P = 0.29$), suggesting a more localized phenomenon instead of generalized outer retinal thickening (Supplementary Table 1). A similar feature has been highlighted in female *RPGR* carriers, where the reflective changes on OCT were described as occurring in the ellipsoid and interdigitation zones.[15,16] Interestingly, the LRP signatures recorded in regions of the tapetal reflex in female *RPGR* carriers resemble those of our male *RPGR* CRD cohort.[15] The precise etiology and cellular location of the abnormal OCT band are both unknown; however, the hyper-reflective changes we identified in our study seem to begin at the EZ interface and extend distally, likely reflecting changes in the photoreceptor basal outer segment discs (Fig. 3A). Consistent with this hypothesis, Kalitzeos et al (2019)[15] correlated the OCT changes with adaptive optics imaging in female *RPGR* carriers and identified hyper-reflective rod outer segments that corresponded to the tapetal-like reflex in the parafoveal region.

Curiously, patients with an atypical form of congenital stationary night blindness called Oguchi disease also manifest remarkably similar OCT features and a corresponding tapetal-like fundus reflex.[21,22,34] Oguchi disease is caused by biallelic pathogenic variants in *SAG* or *GRK1* that result in impaired visual system recovery after photoactivation, particularly in rod photoreceptors.[35,36] The abnormally hyper-reflective outer retinal changes on OCT in Oguchi disease have been demonstrated to normalize after a prolonged period of dark adaptation, correlating with the Mizuo–Nakamura phenomenon observed by fundoscopy.[21,22] Interestingly, we identified a similar change in the OCT appearance in a patient with *RPGR* CRD after the same 2-hour period of dark adaptation (Fig. 6). Although these results must be confirmed in additional patients, the

Investigative Ophthalmology & Visual Science

possibility exists for a potential application of this OCT finding as a biomarker or surrogate for the integrity of dark adaptation. Other published cases of *RPGR* CRD do reveal abnormal hyper-reflective OCT changes,[32,37,38] although the authors do not specifically comment on these features, indicating that these findings represent a more widely present association that includes cohorts outside of our site. Finally, the retinal sheen and OCT reflectivity changes we observed in our cohort also demonstrate similarities to the white-without-pressure (WWOP) and dark-without-pressure (DWOP) phenomena that occur in the midperipheral and far peripheral areas of the fundus.[39,40] The WWOP lesions exhibit increased reflectivity in the EZ, photoreceptor outer segment, and interdigitation zone regions on OCT, whereas DWOP lesions exhibit decreased reflectivity in these regions.[39] Despite the clinical impression that these lesions arise from vitreoretinal interface abnormalities, this has not been confirmed on OCT imaging, suggesting an alternate etiology.[39,40]

The striking similarities in the appearance of the tapetal-like retinal sheen, the presence of the abnormally broad hyper-reflective OCT band, and the normalization of the OCT features after prolonged dark adaptation in both Oguchi disease and *RPGR* CRD suggest that these patients may share a similar pathophysiological mechanism. One possibility is that patients with *RPGR* CRD also have impaired rhodopsin recovery after photoactivation. Rhodopsin is a highly abundant protein in the rod outer segments and has an absorption maximum at 500 nm.[41] If rhodopsin were in a state of inappropriate photoactivation at baseline, the fundus would absorb fewer photons of shorter wavelength, and these photons may instead be reflected. This process could result in a greenish hue on Optos laser imaging and a shift from a reddish-orange to a golden-yellow fundus appearance with full spectrum light owing to the inclusion of shorter wavelengths of reflected light (ie, 500 nm). This factor may explain the tapetal-like retinal sheen evident in our *RPGR* CRD cohort and in other cases such as Oguchi disease. Intriguingly, the rd9 mouse, a bone fide genetic model of human *RPGR*^{ORF15} frameshift mutations, also manifests a yellowish fundus appearance upon exposure to bright light.[42]

Although mitochondrial membranes normally contribute to the reflectivity of the EZ band on OCT,[43] the broadened hyper-reflective band apparent in our *RPGR* CRD cohort extends distal to the EZ interface, likely indicating changes in the basal outer segments. Bleaching of rhodopsin, the most abundant protein in the discs, alters disc membrane morphology and can lead to vesiculation and disorganization, even at a modest 400 lux, potentially accounting for the presence of the broad hyper-reflective band.[44,45] Indeed, rhodopsin bleaching in mice has been shown to cause increased EZ and rod outer segment reflectivity on OCT.[46] Interestingly, Fawzi et al (2014)[39] proposed that the outer retinal reflectivity changes evident on OCT in patients with WWOP and DWOP may arise from regional altered absorption properties of photopigments in the outer segments and related the OCT findings to those present in Oguchi disease. The occurrence of WWOP and DWOP lesions in the midperipheral and far peripheral areas of the retina lends support to our hypothesis that the hyper-reflective OCT band in our cohort arises from surviving rod outer segments in the macula. Although our *RPGR* cohort with the retinal sheen clearly has a cone-dominant disorder, there is definite rod dysfunction on ERG and the distribution of the retinal sheen corresponds to regions of high rod photoreceptor density.[47] Our hypothesis that the retinal sheen and abnormal OCT hyper-reflectivity arise from rod photoreceptors with impaired photoactivation recovery is quite speculative and will require careful validation. The true origin of the retinal sheen in Oguchi disease and our *RPGR* cohort remains to be determined.

Apart from the fundus and OCT similarities, both our *RPGR* cohort with CRD and patients with Oguchi disease retain functionally deficient but structurally intact rods. Recently, a CRD phenotype has been described in patients with biallelic pathogenic variants in *TTLL5*.[24] This gene is expressed in photoreceptors and the resulting protein binds to RPGR at its C-terminal basic domain (BD in Fig. 5) and glutamylates ORF15.[8] The precise consequence of this post-translational modification to RPGR is uncertain, but loss of function of TTLL5 phenocopies *RPGR* CRD in our cohort (Fig. 7). Given that the *RPGR* CRD variants cluster toward the 3′-end of *RPGR*^{ORF15} just upstream of the basic domain (Fig. 5), one hypothesis is that these variants produce an RPGR transcript that escapes nonsense-mediated mRNA decay and may still result in a partially functional protein that lacks its basic domain. This factor could explain the relative preservation of some rod function in patients with variants in *RPGR* toward the 3′-end of ORF15 and might indicate that the cone dysfunction in *RPGR* CRD has a shared underlying disease mechanism with TTLL5.

When comparing the groups with and without the retinal sheen and OCT changes (Table 2), we did not identify a significant difference in mean logMAR visual acuity. Patients with *RPGR* CRD have been shown to have a higher likelihood of having poorer central acuity than *RPGR* RCD patients at a given age.[9] In our study, because the retinal sheen was predominantly evident in a parafoveal distribution, visual acuity may not be the most sensitive measure to use for comparison as it reflects the status of the fovea. Future studies using multifocal ERG or pattern ERG may be more revealing.

In the *RPGR* cohort, there were six patients who had a CRD phenotype but did not have a detectable retinal sheen or OCT hyper-reflectivity (Table 2). Four of these patients were heterozygous females and two were hemizygous males. One of the males had a de novo variant *RPGR*:c.2454_2455ins (259 bp), (p.V819Rfs*7), but he lacked the foveal hypoautofluorescence evident in the majority of other *RPGR* CRD patients. Splice-altering pathogenic variants in exon 3 of *OPN1LW* and *OPN1MW* were also identified in his case, presumably providing an alternate etiology for his X-linked CRD. In addition, his *RPGR* variant is more 5′ than most other variants identified in our cohort. The second male who had a CRD phenotype without the retinal sheen had the pathogenic variant *RPGR*:c.3096_3097del. His fundus autofluorescence pattern revealed significant hypoautofluorescent areas along the vascular arcades and nasal to the optic nerve, unlike the other patients with *RPGR* CRD. Importantly, his mother (patient 9) had a tapetal-like retinal sheen and OCT hyper-reflectivity with a normal ERG (Table 1). It is possible that a second genetic change or modifier may account for this discrepancy. Additionally, a subtle retinal sheen or areas of abnormal outer retinal hyper-reflectivity may have indeed existed but were not readily apparent on available fundus or OCT imaging. This latter suggestion may explain why a retinal sheen or OCT changes were not detected in four females with CRD, who might be anticipated to have a

Investigative Ophthalmology & Visual Science

less prominent retinal sheen and OCT changes based on their heterozygous status compared with hemizygous males with CRD.

Although we have identified a tapetal-like retinal sheen and corresponding OCT hyper-reflectivity in a number of patients with *RPGR* CRD, one of the limitations of our study is that it was not always possible to completely mask the expert examiner to the additional features present that could reveal confounding information. The distribution of the outer retinal thinning on OCT was inevitably often revealing and might have introduced bias. However, our quantitative analyses of the LRP of these OCTs provides objective differences of the differences in OCT reflectivity. Future analyses of these OCT and fundus reflex features in prospective cohorts of *RPGR* patients will be important to further validate our findings.

In addition, because the retinal sheen was not apparent in regions where there was frank loss of the EZ, the degree of outer retinal atrophy is an important consideration and may account for the phenotypic discordance between *RPGR* RCD and CRD patients. The presence of intact rods is likely required to visualize the abnormal hyper-reflectivity on OCT. It is possible that the RCD phenotype manifests a similar tapetal-like retinal sheen very early in the disease course. Given the relatively rapid rate of rod photoreceptor loss, by the time most patients with *RPGR*-related RCD present for clinical evaluation, there is already significant outer retinal thinning that limits the ability to detect any potentially abnormal hyper-reflectivity on OCT.

In summary, we report the presence of a tapetal-like retinal sheen and corresponding abnormally broad hyper-reflective outer retinal changes on OCT in nearly one fifth of our *RPGR* cohort. The vast majority of cases were male with a CRD phenotype and had variants toward the 3′-end of *RPGR*^{ORF15}. Neither the retinal sheen nor the hyper-reflective OCT changes were identified in any patients with the RCD phenotype. Our findings indicate that patients with *RPGR* CD or CRD have a generalized phenotype consisting of (1) a tapetal-like retinal sheen, (2) an abnormally broad hyper-reflective EZ band on OCT, and, in hemizygous males, (3) a bullseye pattern of foveal hypoautofluorescence with a surrounding rim of hyperautofluorescence. Importantly, the degree to which these features manifest clinically may depend on the extent of retinal degeneration and disease progression. The change in the appearance of the abnormal outer retinal band on OCT following a period of prolonged dark adaptation raises the possibility of a relative state of impaired inactivation of phototransduction. Further, the phenotype of this *RPGR* CRD group shares strikingly similar findings with *TTLL5*. Together, these features demonstrate insights into the pathobiology of *RPGR*^{ORF15} retinopathy. Further quantification and objective evaluation of these findings could lead to improved diagnostic accuracy and disease categorization as well as present potential outcome measures and may thus have implications in future clinical trials in *RPGR*-related CD/CRD retinopathy.

Acknowledgments

This work was presented at the Association for Research in Vision and Ophthalmology (ARVO) Annual Meeting 2022 in Denver, Colorado, May 4, 2022.

Disclosure: **M.D. Benson**, None; **S. Mukherjee**, None; **A.R. Agather**, None; **D. Blain**, None; **D. Cunningham**, None; **R. Mays**, None; **X. Sun**, None; **T. Li**, None; **R.B. Hufnagel**, None; **B.P. Brooks**, None; **L.A. Huryn**, None; **W.M. Zein**, None; **C.A. Cukras**, None

References

1. Tuupanen S, Gall K, Sistonen J, et al. Prevalence of RPGR-mediated retinal dystrophy in an unselected cohort of over 5000 patients. *Transl Vis Sci Technol*. 2022;11(1):6.
2. Vervoort R, Lennon A, Bird AC, et al. Mutational hot spot within a new RPGR exon in X-linked retinitis pigmentosa. *Nat Genet*. 2000;25(4):462–466.
3. Roepman R, Bernoud-Hubac N, Schick DE, et al. The retinitis pigmentosa GTPase regulator (RPGR) interacts with novel transport-like proteins in the outer segments of rod photoreceptors. *Hum Mol Genet*. 2000;9(14):2095–2105.
4. Linari M, Ueffing M, Manson F, Wright A, Meitinger T, Becker J. The retinitis pigmentosa GTPase regulator, RPGR, interacts with the delta subunit of rod cyclic GMP phosphodiesterase. *Proc Natl Acad Sci USA*. 1999;96(4):1315–1320.
5. Chang B, Khanna H, Hawes N, et al. In-frame deletion in a novel centrosomal/ciliary protein CEP290/NPHP6 perturbs its interaction with RPGR and results in early-onset retinal degeneration in the rd16 mouse. *Hum Mol Genet*. 2006;15(11):1847–1857.
6. Hosch J, Lorenz B, Stieger K. RPGR: role in the photoreceptor cilium, human retinal disease, and gene therapy. *Ophthalmic Genet*. 2011;32(1):1–11.
7. Megaw RD, Soares DC, Wright AF. RPGR: its role in photoreceptor physiology, human disease, and future therapies. *Exp Eye Res*. 2015;138:32–41.
8. Sun X, Park JH, Gumerson J, et al. Loss of RPGR glutamylation underlies the pathogenic mechanism of retinal dystrophy caused by TTLL5 mutations. *Proc Natl Acad Sci USA*. 2016;113(21):E2925–2934.
9. Talib M, van Schooneveld MJ, Thiadens AA, et al. Clinical and genetic characteristics of male patients with RPGR-associated retinal dystrophies: a long-term follow-up study. *Retina*. 2019;39(6):1186–1199.
10. Sandberg MA, Rosner B, Weigel-DiFranco C, Dryja TP, Berson EL. Disease course of patients with X-linked retinitis pigmentosa due to RPGR gene mutations. *Invest Ophthalmol Vis Sci*. 2007;48(3):1298–1304.
11. Ebenezer ND, Michaelides M, Jenkins SA, et al. Identification of novel RPGR ORF15 mutations in X-linked progressive cone-rod dystrophy (XLCORD) families. *Invest Ophthalmol Vis Sci*. 2005;46(6):1891–1898.
12. Flaxel CJ, Jay M, Thiselton DL, et al. Difference between RP2 and RP3 phenotypes in X linked retinitis pigmentosa. *Br J Ophthalmol*. 1999;83(10):1144–1148.
13. Acton JH, Greenberg JP, Greenstein VC, et al. Evaluation of multimodal imaging in carriers of X-linked retinitis pigmentosa. *Exp Eye Res*. 2013;113:41–48.
14. Bregnhøj J, Al-Hamdani S, Sander B, Larsen M, Schatz P. Reappearance of the tapetal-like reflex after prolonged dark adaptation in a female carrier of RPGR ORF15 X-linked retinitis pigmentosa. *Mol Vis*. 2014;20:852–863.
15. Kalitzeos A, Samra R, Kasilian M, et al. Cellular imaging of the tapetal-like reflex in carriers of RPGR-associated retinopathy. *Retina*. 2019;39(3):570–580.
16. Kilgore DA, Kilgore TA, Sukpraprut-Braaten S, Schaefer GB, Uwaydat SH. Multimodal imaging of an RPGR carrier female. *Ophthalmic Genet*. 2021;42(3):312–316.
17. van Osch L, van Schooneveld M, Bleekerwagemakers EM. Golden tapetal reflex in male patients with X-linked retinitis pigmentosa. Case report and practical implications. *Ophthalmic Paediatr Genet*. 1990;11(4):287–291.

18. Schulze-Bonsel K, Feltgen N, Burau H, Hansen L, Bach M. Visual acuities "hand motion" and "counting fingers" can be quantified with the Freiburg Visual Acuity Test. *Invest Ophthalmol Vis Sci*. 2006;47(3):1236–1240.
19. McCulloch DL, Marmor MF, Brigell MG, et al. ISCEV standard for full-field clinical electroretinography (2015 update). *Doc Ophthalmol*. 2015;130(1):1–12.
20. Biegel AC. Oguchi's disease; a case report. *Am J Ophthalmol*. 1955;39(3):405–407.
21. Takada M, Otani A, Ogino K, Yoshimura N. Spectral-domain optical coherence tomography findings in the Mizuo-Nakamura phenomenon of Oguchi disease. *Retina*. 2011;31(3):626–628.
22. Godara P, Cooper RF, Sergouniotis PI, et al. Assessing retinal structure in complete congenital stationary night blindness and Oguchi disease. *Am J Ophthalmol*. 2012;154(6):987–1001.
23. Foote KG, De la Huerta I, Gustafson K, et al. Cone spacing correlates with retinal thickness and microperimetry in patients with inherited retinal degenerations. *Invest Ophthalmol Vis Sci*. 2019;60(4):1234–1243.
24. Sergouniotis PI, Chakarova C, Murphy C, et al. Biallelic variants in TTLL5, encoding a tubulin glutamylase, cause retinal dystrophy. *Am J Hum Genet*. 2014;94(5):760–769.
25. Demirci FY, Rigatti BW, Wen G, et al. X-linked cone-rod dystrophy (locus COD1): identification of mutations in RPGR exon ORF15. *Am J Hum Genet*. 2002;70(4):1049–1053.
26. Sharon D, Sandberg MA, Rabe VW, Stillberger M, Dryja TP, Berson EL. RP2 and RPGR mutations and clinical correlations in patients with X-linked retinitis pigmentosa. *Am J Hum Genet*. 2003;73(5):1131–1146.
27. Heckenlively JR, Weleber RG. X-linked recessive cone dystrophy with tapetal-like sheen. A newly recognized entity with Mizuo-Nakamura phenomenon. *Arch Ophthalmol*. 1986;104(9):1322–1328.
28. Jacobson DM, Thompson HS, Bartley JA. X-linked progressive cone dystrophy. Clinical characteristics of affected males and female carriers. *Ophthalmology*. 1989;96(6):885–895.
29. Bartley J., Gies C., Jacobson D. Cone dystrophy (X-linked) (COD1) maps between DXS7(L1.28) and DXS206(XJ1.1) and is linked to DXS84(754). (Abstract). *Cytogenet Cell Genet*. 51: 959.
30. Hong HK, Ferrell RE, Gorin MB. Clinical diversity and chromosomal localization of X-linked cone dystrophy (COD1). *Am J Hum Genet*. 1994;55(6):1173–1181.
31. Gill JS, Georgiou M, Kalitzeos A, Moore AT, Michaelides M. Progressive cone and cone-rod dystrophies: clinical features, molecular genetics and prospects for therapy. *Br J Ophthalmol*. 2019;103(5):711–720.
32. De Silva SR, Arno G, Robson AG, et al. The X-linked retinopathies: physiological insights, pathogenic mechanisms, phenotypic features and novel therapies. *Prog Retin Eye Res*. 2021;82:100898.
33. Nguyen XT, Talib M, van Schooneveld MJ, et al. RPGR-associated dystrophies: clinical, genetic, and histopathological features. *Int J Mol Sci*. 2020;21(3):835.
34. Kato Y, Tsunoda K, Fujinami K, Iwata T, Saga M, Oguchi Y. Association of retinal artery and other inner retinal structures with distribution of tapetal-like reflex in Oguchi's disease. *Invest Ophthalmol Vis Sci*. 2015;56(4):2162–2172.
35. Fuchs S, Nakazawa M, Maw M, Tamai M, Oguchi Y, Gal A. A homozygous 1-base pair deletion in the arrestin gene is a frequent cause of Oguchi disease in Japanese. *Nat Genet*. 1995;10(3):360–362.
36. Cideciyan AV, Zhao X, Nielsen L, Khani SC, Jacobson SG, Palczewski K. Null mutation in the rhodopsin kinase gene slows recovery kinetics of rod and cone phototransduction in man. *Proc Natl Acad Sci USA*. 1998;95(1):328–333.
37. Mawatari G, Fujinami K, Liu X, et al. Clinical and genetic characteristics of 14 patients from 13 Japanese families with *RPGR*-associated retinal disorder: report of eight novel variants. *Hum Genome Var*. 2019;6:34.
38. Nassisi M, De Bartolo G, Mohand-Said S, et al. Retrospective natural history study of *RPGR*-related cone- and cone-rod dystrophies while expanding the mutation spectrum of the disease. *Int J Mol Sci*. 2022;23(13):7189.
39. Fawzi AA, Nielsen JS, Mateo-Montoya A, et al. Multimodal imaging of white and dark without pressure fundus lesions. *Retina*. 2014;34(12):2376–2387.
40. Yu H, Luo H, Zhang X, et al. Analysis of white and dark without pressure in a young myopic group based on ultra-wide swept-source optical coherence tomography angiography. *J Clin Med*. 2022;11(16):4830.
41. Hubbard R. Absorption spectrum of rhodopsin: 500 nm absorption band. *Nature*. 1969;221(5179):432–435.
42. Thompson DA, Khan NW, Othman MI, et al. Rd9 is a naturally occurring mouse model of a common form of retinitis pigmentosa caused by mutations in RPGR-ORF15. *PLoS One*. 2012;7(5):e35865.
43. Litts KM, Zhang Y, Freund KB, Curcio CA. Optical coherence tomography and histology of age-related macular degeneration support mitochondria as reflectivity sources. *Retina*. 2018;38(3):445–461.
44. Liebman PA, Jagger WS, Kaplan MW, Bargoot FG. Membrane structure changes in rod outer segments associated with rhodopsin bleaching. *Nature*. 1974;251(5470):31–36.
45. Hafezi F, Marti A, Munz K, Remé CE. Light-induced apoptosis: differential timing in the retina and pigment epithelium. *Exp Eye Res*. 1997;64(6):963–970.
46. Zhang P, Goswami M, Zawadzki RJ, Pugh EN The photosensitivity of rhodopsin bleaching and light-induced increases of fundus reflectance in mice measured in vivo with scanning laser ophthalmoscopy. *Invest Ophthalmol Vis Sci*. 2016;57(8):3650–3664.
47. Curcio CA, Sloan KR, Kalina RE, Hendrickson AE. Human photoreceptor topography. *J Comp Neurol*. 1990;292(4):497–523.

Investigative Ophthalmology & Visual Science